Tunable electronic and magnetic properties of WS2 nanoribbons

Hui Zhang, Xi-Bo Li, and Li-Min Liu

Citation: Journal of Applied Physics **114**, 093710 (2013); doi: 10.1063/1.4820470
View online: http://dx.doi.org/10.1063/1.4820470
View Table of Contents: http://scitation.aip.org/content/aip/journal/jap/114/9?ver=pdfcov
Published by the AIP Publishing

Tunable electronic and magnetic properties of WS_2 nanoribbons

Hui Zhang,[1,2] Xi-Bo Li,[2,3] and Li-Min Liu[2,a)]
[1]*Normal College, Shenyang University, Shenyang 110044, China*
[2]*Beijing Computational Science Research Center, Beijing 100084, China*
[3]*Chengdu Green Energy and Green Manufacturing Technology R&D Center, Chengdu, Sichuan, 610207, China*

(Received 17 July 2013; accepted 20 August 2013; published online 6 September 2013)

Two dimensional transition metal dichalcogenides (TMDs) have attracted great attention because of the versatile electronic structures. The electronic and magnetic properties of the nanoribbons are still not fully understood, which are crucial for their applications in nanodevices. In this work, the detailed atomic structural, electronic, and magnetic properties of the one dimensional WS_2 nanoribbons have been carefully explored by first-principles calculations. The results suggest that the single layer WS_2 will first transform into direct band gap semiconductor from indirect band gap of bulk one. Interestingly, the properties of WS_2 nanoribbons are greatly affected by the type of the edges: Armchair nanoribbons (ANRs) remain nonmagnetic and semiconducting as that of bulk, whereas zigzag nanoribbons (ZNRs) exhibit ferromagnetic and metallic. Further, the electronic properties can be tuned by applying the external strains to WS_2 nanoribbons: Band gap of ANRs experiences a direct-indirect-direct transition and the magnetic moment of ZNRs can be easily tuned by the different strains. All these findings suggest that the TMDs nanoribbons may exhibit extraordinary electronic and magnetic properties, and more importantly, such fascinating characters can be precisely modulated by controlling the edge types and applied strains. © *2013 AIP Publishing LLC*. [http://dx.doi.org/10.1063/1.4820470]

I. INTRODUCTION

The discovery[1] of single-layer graphene in 2004 by Novoselov and Geim has shown that it is possible to exfoliate stable, single-layer materials from van der Waals (vdW) solids, which stimulates the research of many other inorganic layered materials.[2,3] The prosperous investigations have focused on low-dimensional materials, such as two-dimensional (2D) graphene, *h*-BN,[4,5] and one-dimensional (1D) nanoribbons.[6,7] In particular, transition metal dichalcogenides (TMDs) have received significant attention because of their unique structures.[8] First, depending on the different combination of chalcogen (such as S and Se) and transition metal (such as Mo, Nb, and V), TMDs contain more than 40 different categories.[9] Second, single-layer TMDs are no longer single-atom thick as in graphene but consisting of transition metal atoms (M) sandwiched between two layers of chalcogen atoms (X) with stoichiometry MX_2. As a result, TMDs possess versatile electronic structure varying from metallic (e.g., VS_2) and semiconducting (e.g., MoS_2) behavior.[10,11]

Among dozens of TMDs, MoS_2 and WS_2 have been extensively studied. The MoS_2 and WS_2 nanosheets have been successfully synthesized through various methods including exfoliation[12–14] and growth.[15] The surface-functionalized WS_2 nanosheets have been synthesized, which can be used as Li-ion battery anodes.[16] Both MoS_2 and WS_2 can be fabricated as high-performance field-effect transistors.[17,18] In addition, MoS_2 can be also used in hydrogen production from water[19–22] and rechargeable batteries.[23] Strong enhancement in photoluminescence (PL) quantum yield is observed for monolayer WS_2 due to exciton recombination at the direct band edge.[24] In contrast to either MoS_2 or WS_2 bilayers, the MoS_2-WS_2 bilayer heterostructure has a direct band gap and more importantly the electron-holes pairs are spatially separated on different monolayers.[25] Besides, the structure and tunable band-gap of mixing $Mo_{1-x}W_xS_2$ single layers have also been characterized recently.[26,27]

The tremendous studies on low-dimensional materials have shown that they may exhibit extraordinary properties compared with their bulk. For carbon-based materials, the 2D graphene has unusual Dirac fermions due to quantum confinement,[28] but energy gaps arise in 1D graphene nanoribbons (GNRs).[29] A strong width-dependent carrier mobility of GNRs has been uncovered by theoretical calculations.[30] Recently, a novel two-dimensional carbon allotrope with tetra-rings and acetylenic linkages, rectangular graphyne (R-graphyne) has been proposed. In addition, half-integer oscillation between metallic state with Dirac-like fermions and semiconductor states occurs in zigzag nanoribbons.[31] For TMDs, an indirect-direct-gap transition occurs in MoS_2 and WS_2 when the system becomes thin from 3D bulk to 2D single-layer, as confirmed by both experiments[32] and theoretical calculations.[33] The MoS_2 Zigzag nanoribbons have a remarkably enhanced binding interaction with Li, compared with the bulk MoS_2 due to the presence of unique edge states, and thus are promising cathode materials for Li-ion batteries.[34]

The previous discussion demonstrated that the low-dimension materials can exhibit a lot of unusual physical phenomena absent in 3D bulk ones. Although both the 3D bulk and 2D single-layer MoS_2 and WS_2 have been widely

a)Email: limin.liu@csrc.ac.cn

studied,[35,36] 1D nanoribbons may exhibit different behavior. In experimental side, ultra-narrow 1D MoS_2 and WS_2 nanoribbons, ~1–4 nm, have been successfully synthesized by using carbon nanotubes as templates.[37,38] In theoretical side, the electronic and magnetic properties of MoS_2 nanoribbons have been predicted to be different from their 3D and 2D structures because of the quantum confinement and edge effects,[39] and can also be modulated by both external strain and electric field engineering.[40–43] The knowledge of 1D WS_2 nanoribbons is also critical for designing WS_2-based nanodevices.

In this work, the electronic and magnetic properties of 1D WS_2 nanoribbons with both armchair and zigzag edges are systematically explored by first-principles calculations. The results demonstrate that both the electronic and magnetic properties of WS_2 nanoribbons are significantly affected by the type of the edge. The WS_2 armchair nanoribbons (ANRs) remain the nonmagnetic and semiconducting behavior of the periodic single-layer one. Contrary to the ANRs, WS_2 zigzag nanoribbons (ZNRs) exhibit the unusual ferromagnetic and metallic behavior introduced by the existence of edges. Fascinatingly, these features of ANRs and ZNRs can be dramatically modulated by applying the external strains along the periodic direction. As the applied strains increase, a direct-indirect-direct transition occurs in ANRs, and the magnetic moment of ZNRs changes step by step. All these findings reveal that both the electronic and magnetic properties of WS_2 nanoribbons can be precisely modulated by controlling the edge type and applied strains, which is crucial for applications in nanodevices.

II. METHODOLOGY

In this work, all calculations were performed based on density functional theory (DFT) with the Vienna *Ab Initio* Simulation Package (VASP).[44,45] Projector-augmented-wave (PAW) potentials[46] were used to account electron-ion interactions. The generalized gradient approximation (GGA) with the Perdew-Burke-Ernzerhof (PBE) functional[47] was used to treat the electron exchange correlation interactions. To remove spurious interactions between neighboring structures due to periodic calculations, a vacuum layer thickness larger than 10 Å was taken. The energy cutoff was set to 400 eV. The Brillouin zone (BZ) was sampled with the Monkhorst-Pack scheme.[48] As for k-point, $15 \times 15 \times 1$ for 2D single-layer WS_2, $8 \times 1 \times 1$ for armchair nanoribbons, and $15 \times 1 \times 1$ for zigzag nanoribbons were adopted, respectively. The equilibrium geometries were fully optimized with both the lattice vectors and atom coordinates relaxed with the tolerance of less than 0.01 eV/Å on each atom.

III. RESULTS AND DISCUSSION

The single-layer WS_2 has graphene-like 2D hexagonal lattice, referred as H-WS_2. As shown in Fig. 1(a), the H-WS_2 exhibits a trigonal prismatic structure with a W atom layer sandwiched by two S atom layers with the sequence of S-W-S. The single-layer H-WS_2 belongs to P-6M2(D_{3h}) point group symmetry, and three atoms in unit cell, one W atom in Wyckoff site *1(a)* at (0, 0, 0) and two S atoms in *2(h)* at (1/3, 2/3, ±Z) in the unit cell. Two types of WS_2 nanoribbons (NRs) can be constructed by cutting the single-layer WS_2 along the different directions. As shown in Figs. 1(b) and 1(c),ANR and ZNR are distinguished due to distinct shaped edges. In the following, the WS_2 nanoribbons are abbreviate as A_n or Z_n, where letters A and Z represent armchair and zigzag edges, and the index number n stands for the width given by the number of WS_2 units contained in primitive cell of A_n and Z_n, respectively. The width of A_n (Z_n) can be simply described by N_A (N_Z), where N_A equals to the index n in A_n (Z_n). In addition, the ideal ribbon width of A_n or Z_n can be also approximately estimated from the lattice constant of single-layer WS_2, a_{SL}, as $W_A = (N_A - 1) \times a_{SL}/2$, and $W_Z = (N_Z - 1) \times 1.732 \times a_{SL}/2$. As discussed below, the

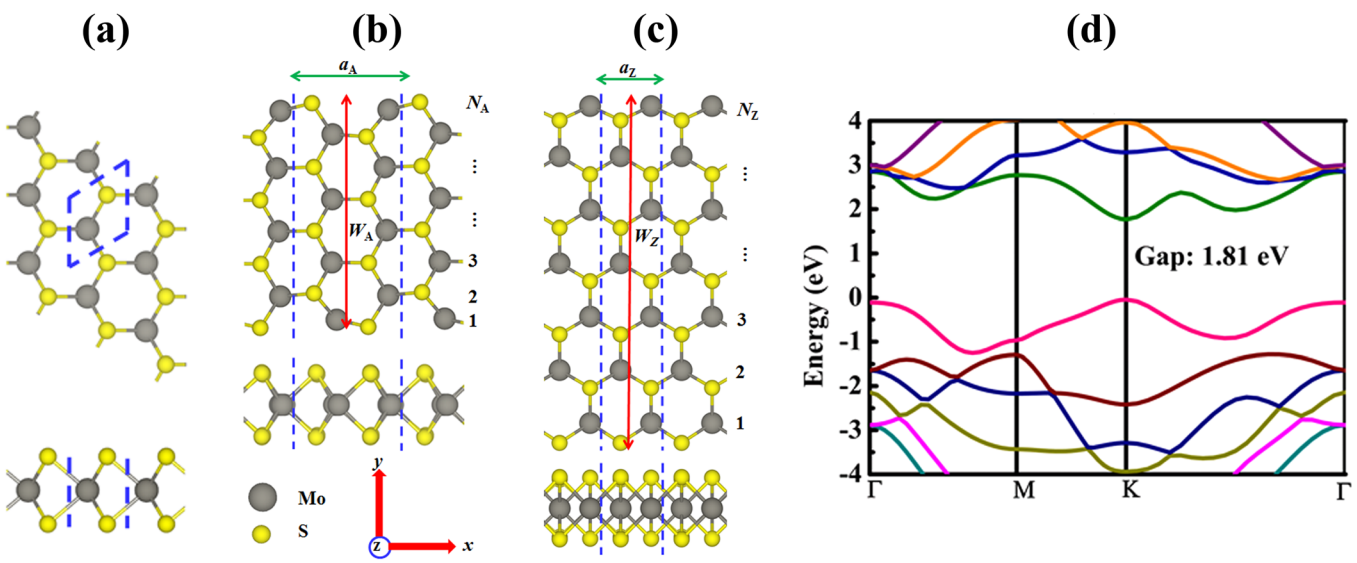

FIG. 1. Atomic structure of 2D periodic single-layer WS_2 (a) and 1D nanoribbons: armchair (b) and zigzag (c) nanoribbons. In (a)–(c), the upper and down views are shown on top and side panel, respectively. The gray (yellow) balls stand for W (S) atoms. The unit cells are depicted by the blue dashed lines. The lattice constants a_A and a_Z of ANRs and ZNRs are indexed by green arrows, whereas the width W_A and W_Z of ANRs and ZNRs are depicted by red arrows, which are also described by N_A and N_Z, respectively. The band structure of single-layer WS_2 is shown in (d).

structure and electronic properties of A_8 and Z_7 can basically describe well the properties of armchair and zigzag type nanoribbons. In the following, we mainly focus on these two representative WS_2 nanoribbons.

The calculated lattice constant of single-layer WS_2 is $a_{SL} = 3.18$ Å, the corresponding W-S bond length is 2.42 Å, and thickness of S-W-S layer (the distance of two S atom planes) is 3.14 Å. The calculated lattice constant, a_{SL}, agrees well with the previous results, 3.13 Å[49] from the local density approximation (LDA) and 3.18 Å[50] from DFT-PBE. The calculated lattice constant of WS_2 nanoribbons is $a_A = 5.47$ Å for A_8, and $a_Z = 3.15$ Å for Z_7. The ideal lattice constants are $a_A = 1.732^* a_{SL} = 5.51$ Å and $a_Z = a_{SL} = 3.18$ Å. The structure parameters of ANRs and ZNRs change slightly after the structure optimization. The calculated band structure of single-layer WS_2 is shown in Fig. 1(d), The single-layer WS_2 has a direct band gap of 1.81 eV according to the present DFT-PBE calculation, which agrees well the previous value of 1.98 eV by DFT-LDA.[49]

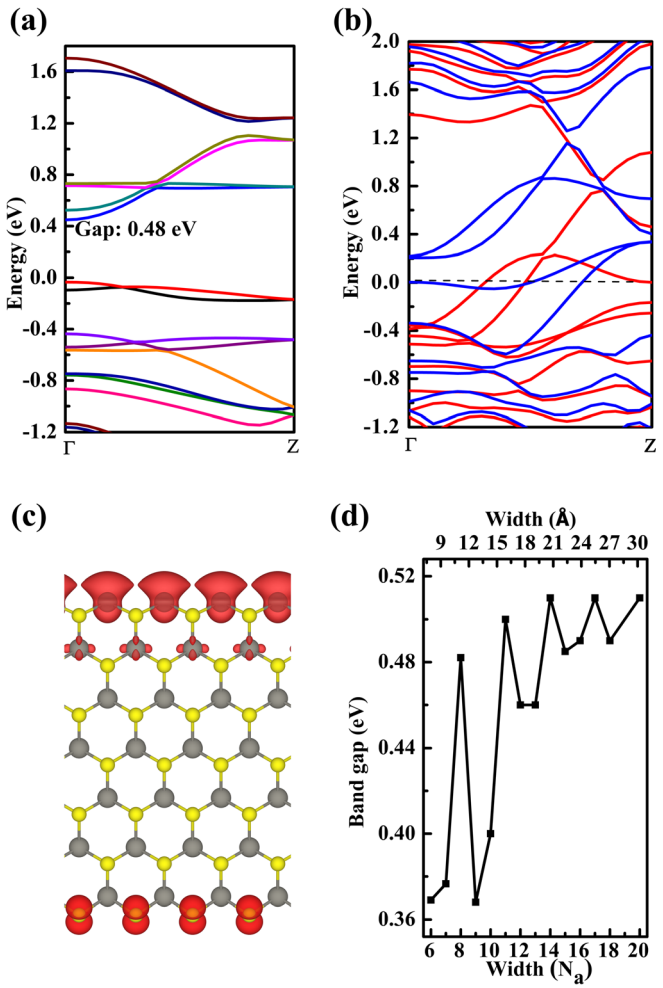

FIG. 2. Band structures of (a) A_8 and Z_7 (b). In (a), different colors represent various bands, whereas in (b), the red and blue represent the spin-up and spin-down bands, respectively. (c) The net spin density distribution on each atom of Z_7, where the red represents the positive density, which is calculated by the difference between the density of spin-up and spin-down states. (d) The band gap of ANRs as a function of ribbon width. The bottom and top axes represent the ribbon width given in N_A (the number of WS_2 units contained in unit cell) and in angstrom, respectively.

In order to understand the detailed electronic properties of 1D nanoribbons, the relationship between electronic structure and width was also checked. As shown in Fig. 2(a), A_8 is semiconducting with a direct band gap. It is noted that the band gap (0.48 eV) for A_8 is only about one-third of the value for single-layer WS_2. The result demonstrated that WS_2 ANRs keep semiconducting independent with the ribbon width. Fig. 2(d) exhibits that the band gaps change with the ribbon width N_A varying from 6 to 20. More interestingly, WS_2 ANRs with $N_A = 3n - 1$ are larger than the neighboring ones with $N_A = 3n - 2$ or $N_A = 3n$, where n is an integer number. The band gaps converge a value of about 0.5 eV when the width is larger than 30 Å, but are still much smaller than that (1.8) eV of single-layer WS_2 due to the edge effect.

As shown above, both 3D bulk and 2D single-layer WS_2 are nonmagnetic semiconductors, herein, the spin-polarization calculations were used to check whether the novel magnetism exists in WS_2 nanoribbons. The spin-polarization calculation on armchair ribbon A_8 gives the same results as that of the spin-unpolarization case, and no magnetic moment is possessed by A_8. Thus, ground state of A_8 is also nonmagnetic. Different from ANRs, spin-polarization calculations are crucial for ZNRs. The total energy indicates that Z_7 prefers to ferromagnetic (FM) state than the nonmagnetic (NM) one by 0.07 eV/cell. As shown in Fig. 2(b), the spin-splitting obviously occurs in Z_7. As shown in Fig. 2(c), the magnetic moment of Z_7 concentrates on the edge atoms. It should be noted that both the two edges of Z_7 possess positive magnetic moment. Thus, WS_2 ZNRs are completely ferromagnetic for both edges. The ferromagnetism of unsaturated edges for WS_2 ZNRs is similar to the case of MoS_2 ZNRs.[39] Besides the magnetism difference of ZNRs and ANRs, there are bands crossing the Fermi energy as depicted in Fig. 2(b), so that WS_2 ZNRs become metallic from semiconducting of 3D bulk and single-layer WS_2. The width effects are also examined in WS_2 ZNRs, and the results show that the ferromagnetic and metallic behavior of the ZNRs does not change with the ribbon width. Interestingly, the magnetic moment of ZNRs changes slightly per unit cell as the increase of width. However, the magnetic moment of ZNRs averaged on WS_2 formula decreases dramatically with the increase of width. It is not difficult to understand that the magnetic moment is ignorable for infinitely width ZNR because the magnetic moment mainly originates from the edge atoms.

It is worth to note that the 2D single-layer periodic WS_2 exhibits nonmagnetic and semiconducting behavior, but novel ferromagnetic and metallic behavior is introduced to ZNRs due to the existence of edges. These different features between WS_2 ANRs and ZNRs demonstrate that both the electronic structure and magnetic properties of WS_2 nanoribbons are significantly affected by the type of the edge.

An essential requirement for material applications in nanoelectronic devices is the ability to modulate the electronic and magnetic properties via external control such as mechanical strains. Next, the strain-effect on electronic and magnetic properties is further investigated for the WS_2 nanoribbons. The external strain is simulated by the variation of the lattice constant along the periodic direction as: $\varepsilon = (a - a_0)/a_0$, where a_0 is the full relaxed lattice constant in

unstrained state, whereas a is the strained lattice constant. In this work, only tensile strains ($\varepsilon > 0$) are considered because it is much easier to be applied than compressing ones in experiments. All atoms are fully relaxed with fixed lattice constant under each strain condition.

Interestingly, the band gap of strained armchair ribbon A_8 fluctuates greatly with different strains. As shown in Fig. 3(a), the variation of the band gap can be divided into three different stages in terms of applied strain: 0%–3% (stage I), 3%–10% (stage II), and 12%–16% (stage III). When the strain is small at the beginning (stage I), the band gap increases monotonically with increasing the strain. At the end of this stage, the band gap gradually increases from initial 0.48 eV to 0.50 eV at strain = 3%. As shown in Fig. 3(b), the increase of band gaps in stage I mainly arises from the increase of the conduction band minimum at Γ (CBM-Γ). In addition, the valence band maximum at Z and Γ (VBM-Z and VBM-Γ) crossover together at strain = 3%, and the former begins to exceed the latter. The band gap consequently transforms from a direct gap at Γ-Γ to an indirect band gap at Z-Γ starting from strain = 3% (Fig. 3(d)). For example, the band gap becomes 0.42 eV at strain = 6% (Fig. 3(e)). In stage II, the band structure retains indirect, while the band gap first decreases, then it increases (Fig. 3(b)). In this stage, the energy at VBM-Z does not change, whereas that at CBM-Γ makes the main contribution to the change of band gap. When strain is larger than 10%, the energy at CBM-Z is even lower than that at CBM-Γ. The gaps convert back into direct but at Z-Z instead of at Γ-Γ for unstrained case. The band gap has a sudden drop at strain = 12% relative to that of 10%. After this, the band gap increases monotonously up to 16% (Fig. 3(f)) due to the variation of energy at CBM-Z in stage III. In the whole process, the band structure experiences a direct-indirect-direct transition of ANR band gap.

Another important feature is that both total magnetic moment and the magnetic moment on specified atoms of

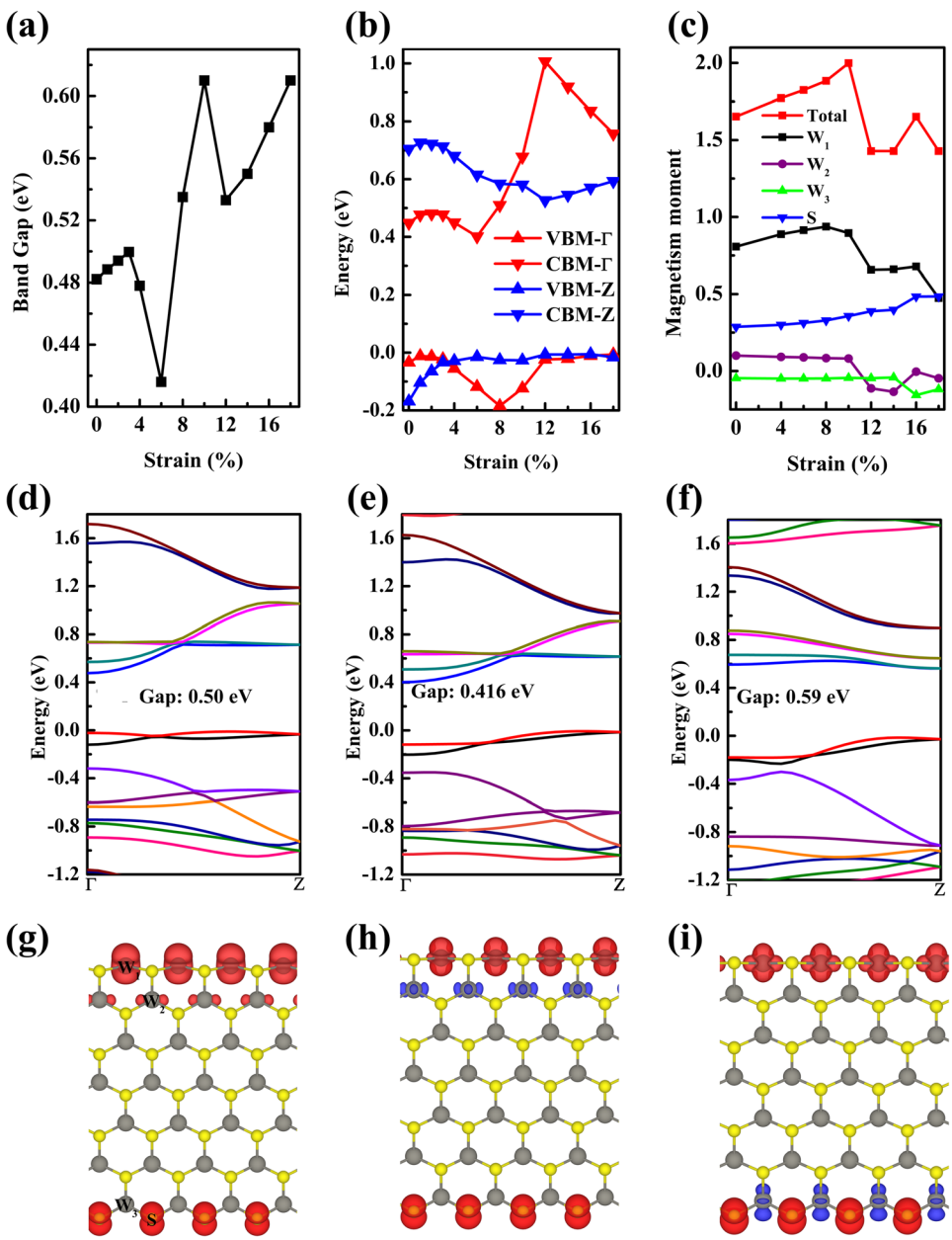

FIG. 3. (a) Band gap, (b) energy variations at Γ and Z of CBM and VBM for A_8, and (c) magnetic moments for Z_7 at various strains. (d)–(f) Band structures of A_8 with strain = 3%, 6%, and 9%, respectively. (g)–(i) The spin density distribution on each atom of Z_7 with strain = 10%, 12%, and 16%, respectively.

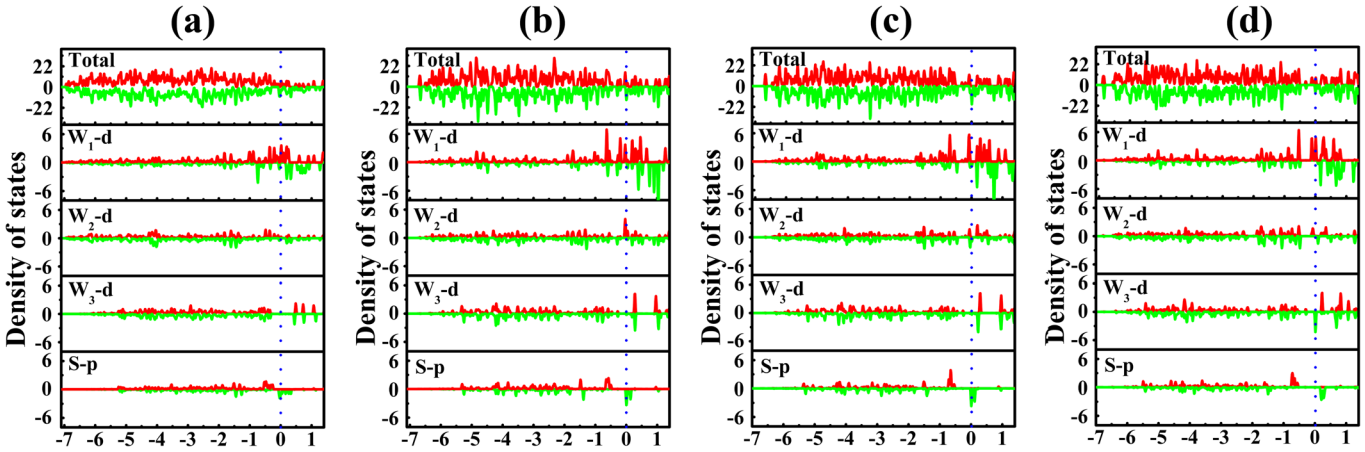

FIG. 4. (a)–(d) TDOS and PDOS for Z7 at strain = 0, %10%, 12%, and 16%, respectively.

ZNRs vary with the applied strains. The magnetic moment on W_2 near the edge is small at the beginning, but it transforms from positive to negative one at strain = 12% (Figs. 3(g) and 3(h)) then decreases to zero at strain = 16%. In this process, another W_2 atom near the opposite edge begins to possess magnetic moment (Fig. 3(i)). Although the magnetic moment on each atom fluctuates with the strains, the magnetic moment is still mainly contributed by edge W and S atoms. The WS_2 ZNR Z_7 possesses the maximum magnetic moment at strain = 10%. The calculations suggest that the magnetic moment of WS_2 nanoribbons can be precisely tuned, which is crucial for applications in magnetic devices, such as a mechanical switch for spin-polarized transport.

To further understand the magnetic property of Z_7 and its variation on strains, the total density of states (TDOS) and projected density of states (PDOS) of specific atoms Z_7 are depicted in Fig. 4. The different atoms are labeled as depicted in Fig. 3(g). The W_1 or S represents the edged W and S atoms, while W_2 and W_3 represent the W atoms close to the edge, respectively. The above analysis shows that zigzag nanoribbons are metallic due to bands crossing the Fermi energy. It should be noted that for unstrained Z_7 only W_1 and S atoms possess electronic density near the Fermi energy (Fig. 4(a)). This indicates that the metallic character of ZNRs mainly arises from the atoms on zigzag edge.

The PDOS also clearly explains the magnetic moment distribution in ZNRs. As shown in Fig. 4(a), the unstrained Z_7 exhibit asymmetric up and down states near the Fermi surface. In addition, the spin-polarization occurs obviously on edge atoms (W_1 and S), and few states on second nearby edge atoms (W_2 and W_3). The different spin-polarization behavior on different atoms is inconsistent with the result that the edge W_1 atom has the largest magnetic moment 0.53 μ_B, the edge S atom has a smaller magnetic moment of 0.32 μ_B, and the other atoms make few contributions to the magnetic moment. These results indicate that both the metallic behavior and magnetic property are induced by the edge atoms. As shown in Figs. 4(b)–4(d), the PDOS on each atom near the Fermi surface changes asymmetrically for spin-up and -down states when strain is applied. For example, no state occurs on W_3 atom when strain is small (Figs. 4(b) and 4(c)), but obvious spin-down state appears at strain = 16% (Fig. 4(d)), which is inconsistent with the fact that W_3 atom possesses no magnetic moment at small strains (Figs. 3(g) and 3(h)), but owns a negative magnetic moment at strain = 16% (Fig. 3(i)). The PDOS (Fig. 4) further confirms the variation of magnetic moment as the strain changes.

IV. CONCLUSIONS

The detailed atomic structure, electronic, and magnetic properties of 1D WS_2 nanoribbons with both armchair and zigzag edges are systematically explored by first-principles calculations. The results demonstrate that the band gap of nanoribbon is dramatically reduced due to the existence of edge compared with the bulk WS_2. Interestingly, the WS_2 armchair nanoribbons retain the nonmagnetic and semiconducting behavior as that of bulk one, while zigzag nanoribbons exhibit the unusual ferromagnetic and metallic behavior. The results suggest that both the electronic and magnetic properties of WS_2 nanoribbons are greatly affected by type of the edge. More importantly, either the electronic or magnetic properties of ANRs and ZNRs can be modulated by applying the external strains. When strain is applied, a direct-indirect-direct transition occurs along with the tunable band gap in ANRs, and the magnetic moment of ZNRs changes step by step. All these findings provide a novel way to effectively tune the electronic and magnetic properties of WS_2 nanoribbons by controlling the edge types and applied strains, which is crucial for applications in electronic devices.

ACKNOWLEDGMENTS

This work was supported by the National Natural Science Foundation of China (No. 51222212), the CAEP foundation (Grant No. 2012B0302052), and the MOST of China (973 Project, Grant No. 2011CB922200). The computations support from Informalization Construction Project of Chinese Academy of Sciences during the 11th Five-Year Plan Period (No. INFO-115-B01) is also highly acknowledged.

[1]K. S. Novoselov, A. K. Geim, S. V. Morozov, D. Jiang, Y. Zhang, S. V. Dubonos, I. V. Grigorieva, and A. A. Firsov, Science **306**, 666 (2004).
[2]M. S. Xu, T. Liang, M. M. Shi, and H. Z. Chen, Chem. Rev. **113**, 3766 (2013).

[3]Y. C. Wang, M. S. Miao, J. Lv, L. Zhu, K. T. Yin, H. Y. Liu, and Y. M. Ma, J. Chem. Phys. **137**, 224108 (2012).
[4]Y. C. Li, P. C. Chen, G. Zhou, J. Li, J. Wu, B.-L. Gu, S. B. Zhang, and W. H. Duan, Phys. Rev. Lett. **109**, 206802 (2012).
[5]L. Song, L. J. Ci, H. Lu, P. B. Sorokin, C. H. Jin, J. Ni, A. G. Kvashnin, D. G. Kvashnin, J. Lou, B. I. Yakobson, and P. M. Ajayan, Nano Lett. **10**, 3209 (2010).
[6]Y.-W. Son, M. L. Cohen, and S. G. Louie, Nature **444**, 347 (2006).
[7]Y. Ding, Y. L. Wang, and J. Ni, Appl. Phys. Lett. **95**, 123105 (2009).
[8]S. Z. Butler, S. M. Hollen, L. Cao, Y. Cui, J. A. Gupta, H. R. Gutierrez, T. F. Heinz, S. S. Hong, J. Huang, A. F. Ismach, E. Johnston-Halperin, M. Kuno, V. V. Plashnitsa, R. D. Robinson, R. S. Ruoff, S. Salahuddin, J. Shan, L. Shi, M. G. Spencer, M. Terrones, W. Windl, and J. E. Goldberger, ACS Nano **7**, 2898 (2013).
[9]M. Chhowalla, H. S. Shin, G. Eda, L.-J. Li, K. P. Loh, and H. Zhang, Nat. Chem. **5**, 263 (2013).
[10]Y. D. Ma, Y. Dai, M. Guo, C. W. Niu, Y. T. Zhu, and B. B. Huang, ACS Nano **6**, 1695 (2012).
[11]K. F. Mak, C. Lee, J. Hone, J. Shan, and T. F. Heinz, Phys. Rev. Lett. **105**, 136805 (2010).
[12]J. N. Coleman, M. Lotya, A. O'Neill, S. D. Bergin, P. J. King, U. Khan, K. Young, A. Gaucher, S. De, R. J. Smith, I. V. Shvets, S. K. Arora, G. Stanton, H. Y. Kim, K. Lee, G. T. Kim, G. S. Duesberg, T. Hallam, J. J. Boland, J. J. Wang, J. F. Donegan, J. C. Grunlan, G. Moriarty, A. Shmeliov, R. J. Nicholls, J. M. Perkins, E. M. Grieveson, K. Theuwissen, D. W. McComb, P. D. Nellist, and V. Nicolosi, Science **331**, 568 (2011).
[13]G. Cunningham, M. Lotya, C. S. Cucinotta, S. Sanvito, S. D. Bergin, R. Menzel, M. S. P. Shaffer, and J. N. Coleman, ACS Nano **6**, 3468 (2012).
[14]H. Li, G. Lu, Y. L. Wang, Z. Y. Yin, C. X. Cong, Q. Y. He, L. Wang, F. Ding, T. Yu, and H. Zhang, Small **9**, 1974 (2013).
[15]S. F. Wu, C. M. Huang, G. Aivazian, J. S. Ross, D. H. Cobden, and X. D. Xu, ACS Nano **7**, 2768 (2013).
[16]R. Bhandavat, L. David, and G. Singh, J. Phys. Chem. Lett. **3**, 1523 (2012).
[17]B. Radisavljevic, A. Radenovic, J. Brivio, V. Giacometti, and A. Kis, Nat. Nanotechnol. **6**, 147 (2011).
[18]D. Braga, I. G. Lezama, H. Berger, and A. Morpurgo, Nano Lett. **12**, 5218 (2012).
[19]A. M. Appel, D. L. DuBois, and R. M. DuBois, J. Am. Chem. Soc. **127**, 12717 (2005).
[20]T. F. Jaramillo, K. P. Jørgensen, J. Bonde, J. H. Nielsen, S. Horch, and I. Chorkendorff, Science **317**, 100 (2007).
[21]H. I. Karunadasa, E. Montalvo, Y. Sun, M. Majda, J. R. Long, and C. J. Chang, Science **335**, 698 (2012).
[22]X. Zong, H. J. Yan, G. P. Wu, G. J. Ma, F. Y. Wen, L. Wang, and C. Li, J. Am. Chem. Soc. **130**, 7176 (2008).
[23]K. Chang and W. X. Chen, ACS Nano **5**, 4720 (2011).
[24]W. J. Zhao, Z. Ghorannevis, L. Q. Chu, M. L. Toh, C. Kloc, P. H. Tan, and G. Eda, ACS Nano **7**, 791 (2013).
[25]K. Kośmider and J. Fernández-Rossier, Phys. Rev. B **87**, 075451 (2013).
[26]D. O. Dumcenco, H. Kobayashi, Z. Liu, Y.-S. Huang, and K. Suenaga, Nature Commun. **4**, 1351 (2013).
[27]Y. F. Chen, J. Y. Xi, D. O. Dumcenco, Z. Liu, K. Suenaga, D. Wang, Z. G. Shuai, Y.-S. Huang, and L. M. Xie, ACS Nano **7**, 4610 (2013).
[28]K. S. Novoselov, A. K. Geim, S. V. Morozov, D. Jiang, M. I. Katsnelson, I. V. Grigorieva, S. V. Dubonos, and A. A. Firsov, Nature **438**, 197 (2005).
[29]Y.-W. Son, M. L. Cohen, and S. G. Louie, Phys. Rev. Lett. **97**, 216803 (2006).
[30]M.-Q. Long, L. Tang, D. Wang, L. J. Wang, and Z. G. Shuai, J. Am. Chem. Soc. **131**, 17728 (2009).
[31]W.-J. Yin, Y.-E. Xie, L.-M. Liu, R.-Z. Wang, X.-L. Wei, L. Lau, J.-X. Zhong, and Y.-P. Chen, J. Mater. Chem. A **1**, 5341 (2013).
[32]H. R. Gutiérrez, N. Perea-López, A. L. Elías, A. Berkdemir, B. Wang, R. Lv, F. López-Urías, V. H. Crespi, H. Terrones, and M. Terrones, Nano Lett. **13**, 3447 (2013).
[33]A. Kuc, N. Zibouche, and T. Heine, Phys. Rev. B **83**, 245213 (2011).
[34]Y. F. Li, D. H. Wu, Z. Zhou, C. R. Cabrera, and Z. F. Chen, J. Phys. Chem. Lett. **3**, 2221 (2012).
[35]H. S. S. R. Matte, A. Gomathi, A. K. Manna, D. J. Late, R. Datta, S. K. Pati, and C. N. R. Rao, Angew. Chem. **122**, 4153 (2010).
[36]Y. D. Ma, Y. Dai, M. Guo, C. W. Niu, J. B. Lu, and B. B. Huang, Phys. Chem. Chem. Phys. **13**, 15546 (2011).
[37]Z. Y. Wang, H. Li, Z. Liu, Z. J. Shi, J. Lu, K. Suenaga, S.-K. Joung, T. Okazaki, Z. N. Gu, J. Zhou, Z. X. Gao, G. P. Li, S. Sanvito, E. Wang, and S. Iijima, J. Am. Chem. Soc. **132**, 13840 (2010).
[38]Z. Y. Wang, K. K. Zhao, H. Li, Z. Liu, Z. J. Shi, J. Lu, K. Suenaga, S.-K. Joung, T. Okazaki, Z. X. Jin, Z. N. Gu, Z. X. Gao, and S. Iijima, J. Mater. Chem. **21**, 171 (2011).
[39]Y. F. Li, Z. Zhou, S. B. Zhang, and Z. F. Chen, J. Am. Chem. Soc. **130**, 16739 (2008).
[40]H. Pan and Y.-W. Zhang, J. Phys. Chem. C **116**, 11752 (2012).
[41]L. Z. Kou, C. Tang, Y. Zhang, T. Heine, C. F. Chen, and T. Frauenheim, J. Phys. Chem. Lett. **3**, 2934 (2012).
[42]K. Dolui, C. D. Pemmaraju, and S. Sanvito, ACS Nano **6**, 4823 (2012).
[43]Q. H. Liu, L. Z. Li, Y. F. Li, Z. X. Gao, Z. F. Chen, and J. Lu, J. Phys. Chem. C **116**, 21556 (2012).
[44]G. Kresse and J. Furthmüller, Phys. Rev. B **54**, 11169 (1996).
[45]G. Kresse and J. Furthmüller, Comput. Mater. Sci. **6**, 15 (1996).
[46]G. Kresse and D. Joubert, Phys. Rev. B **59**, 1758 (1999).
[47]J. P. Perdew, K. Burke, and M. Ernzerhof, Phys. Rev. Lett. **77**, 3865 (1996).
[48]H. J. Monkhorst and J. D. Pack, Phys. Rev. B **13**, 5188 (1976).
[49]C. Ataca, H. Şahin, and S. Ciraci, J. Phys. Chem. C **116**, 8983 (2012).
[50]A. Molina-Sanchez and L. Wirtz, Phys. Rev. B **84**, 155413 (2011).